Kondo-like behavior in magnetic and thermal properties of single-crystal $Tm_5Si_2Ge_2$

J. H. Kim,[1] S. J. Kim,[1] C. I. Lee,[1] M. A. Jung,[1] H. J. Oh,[1,2] Jong-Soo Rhyee,[3] Younghun Jo,[4] Hiroyuki Mitani,[5,6] Hidetoshi Miyazaki,[5] Shin-ichi Kimura,[5,7] and Y. S. Kwon[1,*]

[1]*Department of Physics, Sungkyunkwan University, Suwon 440-746, South Korea*

[2]*Department of Ophthalmic Optics, Masan University, Masan 630-729, Republic of Korea*

[3]*Inorganic Materials Group, Samsung Advanced Institute of Technology, Yong-In 446-712, Republic of Korea*

[4]*Nano Materials Research Team, Korea Basic Science Institute, Daejeon 305-333, Korea*

[5]*UVSOR Facility, Institute for Molecular Science, Okazaki 444-8585, Japan*

[6]*Graduate School of Engineering, Shinshu University, Nagano 380-8553, Japan*

[7]*School of Physical Sciences, The Graduate University for Advanced Studies (SOKENDAI), Okazaki 444-8585, Japan*

(Received 13 November 2009; revised manuscript received 28 January 2010; published 3 March 2010)

A stoichiometric $Tm_5Si_{2.0\pm0.1}Ge_{2.0\pm0.1}$ single crystal was grown using the Bridgeman method and was examined by x-ray diffraction, energy dispersive spectroscopy, magnetization, ac and dc magnetic susceptibilities, specific heat, electrical resistivity, and x-ray photoemission spectroscopy experiments. $Tm_5Si_{2.0\pm0.1}Ge_{2.0\pm0.1}$ was found to crystallize with an orthorhombic Sm_5Ge_4-type structure. The mean valence of Tm ions in $Tm_5Si_{2.0\pm0.1}Ge_{2.0\pm0.1}$ was almost trivalent. The $4f$ states were split by the crystalline electric field. The ground state exhibited long-range antiferromagnetic order along the b axis below 8.01 K with the ferromagnetically coupled magnetic moments in the ac plane, whereas the exited states showed a reduced magnetic moment and magnetic entropy and $-\log T$ behaviors.

DOI: 10.1103/PhysRevB.81.104401 PACS number(s): 72.15.Qm, 75.20.Hr, 65.40.Ba

I. INTRODUCTION

There has been renewed interest in $R_5(Si_xGe_{1-x})_4$ pseudobinary compounds (R=rare-earth metals) with the recent discovery of a giant magnetocaloric effect (MCE) in $Gd_5(Si_xGe_{1-x})_4$ by Pecharsky and Gschneidner.[1–28] This effect has potential applications in magnetic refrigerants. The giant MCE in $Gd_5(Si_xGe_{1-x})_4$ is caused by a first-order magnetic transition that accompanies a martensiticlike structural phase transition.[3,4] This suggests that strong coupling between the magnetic and crystallographic lattices is also responsible for the giant magnetoresistance and strong magnetoelasic effect. Hence, most studies in $R_5(Si_xGe_{1-x})_4$ examined the magnetic and crystallographic structures that are important to determining the origin of the giant MCE.

However, interesting mixed valence states of Yb ions were recently observed in $Yb_5(Si_xGe_{1-x})_4$ alloys: nonmagnetic Yb^{2+} ions are located in the $4c$ sites and one of the $8d$ sites, whereas Yb^{3+} ions are located exclusively in the $8d$ sites.[16] The mixed-valence phenomenon can be mostly found in Ce, Sm, Tm, and Yb compounds and is closely related to the Kondo effect with a high Kondo temperature (T_K), which is caused by the strong hybridization between the $4f$ electron and the conduction electron. Unfortunately, there have not been any studies on the Kondo effect in $Yb_5(Si_xGe_{1-x})_4$ alloys.

The MCE may be adversely affected by the Kondo effect because it can decrease the magnetization and remove the magnetic order. To improve the MCE in $R_5(Si_xGe_{1-x})_4$ alloys, especially R=Ce, Sm, Tm, and Yb, it is important to analyze the magnetic properties affected by the Kondo effect. To investigate the mixed-valence state and the Kondo effect, in this study, a single crystal of $Tm_5Si_2Ge_2$ was grown and the lattice constant, transport, magnetic, thermal properties, and x-ray photoemission spectroscopy (XPS) spectra were examined. The Kondo effect and/or mixed-valence state have been not found in Tm compounds except for TmX (X=S, Se, and Te) (Refs. 29 and 30) and thus it is important to study those in $Tm_5Si_2Ge_2$.

II. EXPERIMENTAL DETAILS

A $Tm_5Si_2Ge_2$ single crystal was grown at 1950 °C in a pure tungsten crucible, which had previously been baked out at 2200 °C, using the Bridgeman method. The tungsten crucible never reacts with the constitutive elements. Because of the high volatility of Tm, the starting materials were sealed in welded tungsten crucible using an electron-beam welder. Some Tm evaporates and might settle somewhere else in the crucible. Therefore Tm, Si, and Ge at a ratio of 5.02:2:2 were used as the starting materials. The crystal had a diameter and length of 10 mm and 12 mm, respectively, and was well cleaved along the ac crystallographic plane. Tm metal (99.9 at. % purity) was obtained from a commercial vendor and contained the following major impurities (in at.%): Fe-0.01, Ca-0.03, Mg-0.01, Ni-0.01, Al-0.01, T-0.01, Si-0.01, C-0.015, O-0.05, and Cl-0.05. The Si and Ge elements (99.999 at. % purity) were also purchased from a commercial vendor. The orientations of the b crystallographic axis and ac plane in the sample were determined using the backscattered Laue method.

The magnetic measurements were performed using a superconducting quantum interference device magnetometer (MPMS XL, Quantum Design). The magnetic susceptibility of the zero magnetic field cooled and magnetic field cooled samples was measured as a function of temperature from 2 to 300 K at H=100 Oe. Isothermal magnetization was measured at 2, 4, and 6 K in a dc magnetic field varying from 0 to 5 T for the zero magnetic field cooled and magnetic field cooled samples. The specific heats of $Tm_5Si_2Ge_2$ and

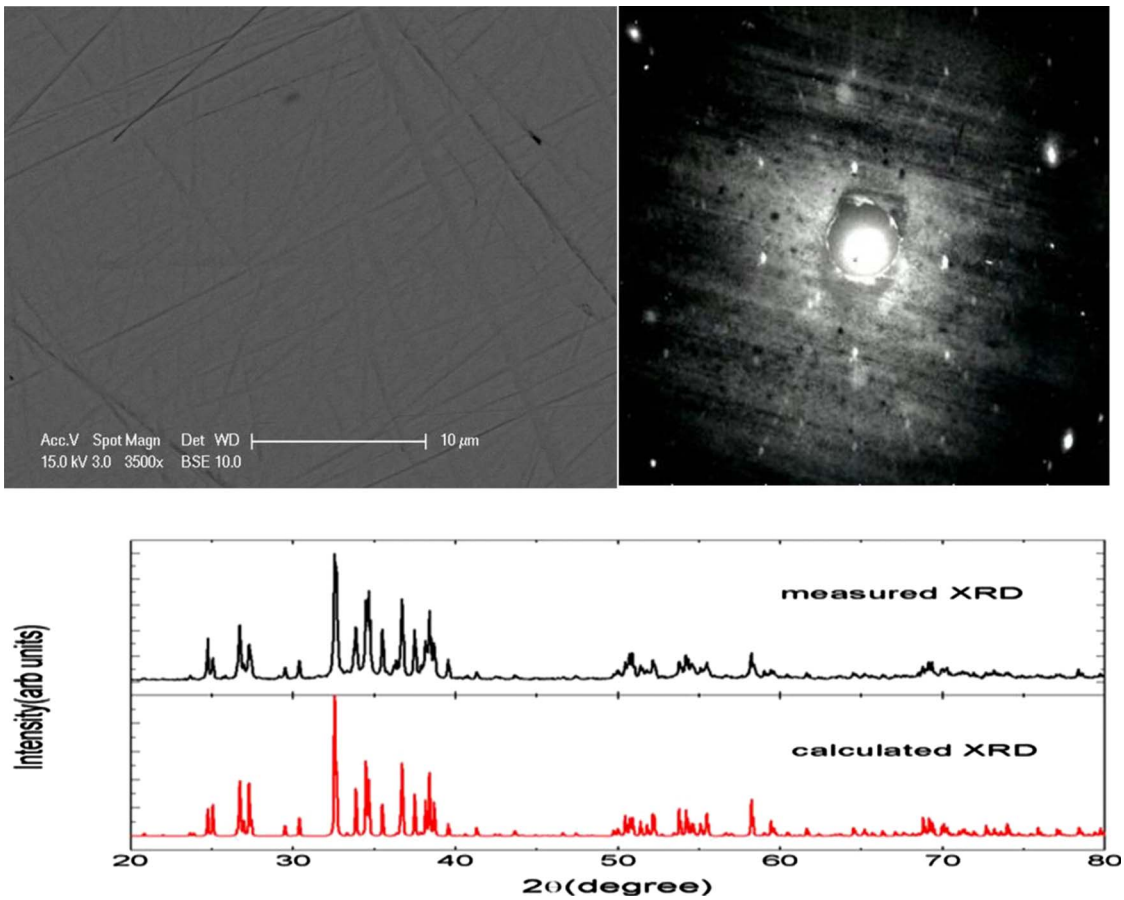

FIG. 1. (Color online) (a) Scanning electron microscopy image of a polished surface of a $Tm_5Si_2Ge_2$ single crystal. (b) Laue diffraction pattern image in the *ac* plane of a $Tm_5Si_2Ge_2$ single crystal. (c) The measured and calculated x-ray diffraction patterns of a $Tm_5Si_2Ge_2$ single crystal.

$Lu_5Si_2Ge_2$ were measured using a physical property measurement system (PPMS, Quantum Design). The former was measured in various magnetic fields, ranging from 0 to 9 T, and oriented parallel to the *b* crystallographic axis.

The mean valence of Tm ions in $Tm_5Si_2Ge_2$ was determined by x-ray photoemission spectroscopy (XPS, Mg $K\alpha$ line, $h\nu=1253.6$ eV) of the Tm 4*d* and 4*p* core levels using a 100 mm radius hemispherical photoelectron analyzer (VG Scienta SES-100). The base pressure of the chamber was less than 2×10^{-8} Pa. The sample temperature and total-energy resolution were set to approximately 20 K and 0.7 eV, respectively. To obtain the mean valence of $Tm_5Si_2Ge_2$, the Tm 4*d* and 4*p* core level XPS spectra of TmS (mostly Tm^{3+}) and TmTe (mostly Tm^{2+}) were also measured for the reference.[29] Clean sample surfaces were prepared inside the ultrahigh-vacuum chamber by scraping with a clean diamond filler. After cleaning, the level of oxygen and carbon contaminations was checked by monitoring the intensity of the O 1*s* and C 1*s* photoemission peaks. The intensities of the O 1*s* and C 1*s* peaks were kept within the noise level during the measurements.

III. EXPERIMENTAL RESULTS AND DISCUSSION

As shown in Fig. 1(a), atomic-number-sensitive backscattered electron imaging of the polished surface of $Tm_5Si_2Ge_2$ single crystal showed that the sample contained a single phase, which was identified as $Tm_5Si_{2.0\pm0.1}Ge_{2.0\pm0.1}$ by energy dispersive spectroscopy. Figure 1(b) shows the imaging of the pattern of Laue diffraction for single-crystal $Tm_5Si_2Ge_2$. The Laue pattern was formed by the x rays diffracted from the *ac* plane of $Tm_5Si_2Ge_2$. Figure 1(c) shows the x-ray diffraction pattern of $Tm_5Si_2Ge_2$. The peaks positions in the pattern are consistent with the diffraction pattern calculated from an orthorhombic Sm_5Ge_4-type crystal structure (space group *Pnma*), which is plotted in Fig. 2, with lattice constants $a=7.455\pm0.001$, $b=14.402\pm0.002$, and $c=7.525\pm0.001$ Å.

Figure 3 shows the change in the lattice parameters of $R_5Si_2Ge_2$ with R=Gd to Lu. $R_5Si_2Ge_2$ is classified into three types of crystal structures, which makes it difficult to deduce the mixed valence of $Tm_5Si_2Ge_2$. It was possible to estimate the valence of *R* ions because the three types of crystal structures are similar and contain four formula units in a unit cell. In R=Gd to Er and Lu, which are trivalent, the lattice parameters and volume of a $R_5Si_2Ge_2$ unit cell decrease smoothly with increasing atomic number due to lanthanide contraction. In the case of R=Tm, the lattice parameters and unit-cell volume were on the line indicating that Tm ion is trivalent. This is inconsistent with results of the magnetic susceptibility and magnetization mentioned below. It should

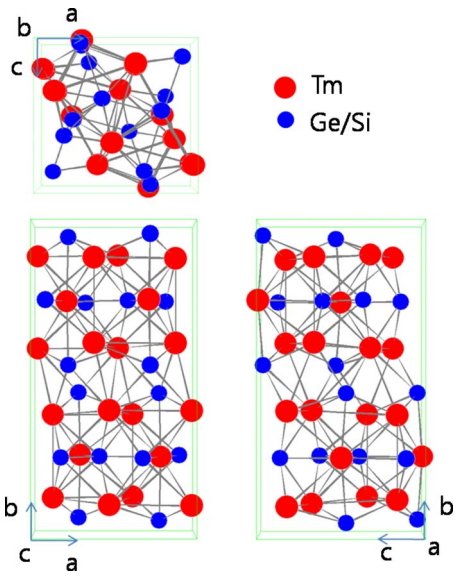

FIG. 2. (Color online) Orthorhombic Sm_5Ge_4-type crystal structure with the space group *Pnma*.

be noted that the unit-cell volume for R=Yb is larger than that indicated by the line formed by the trivalent R ion, which means that Yb ions have an intermediate valence, as reported in Ref. 16.

Figure 4 shows the temperature dependence of the dc magnetic susceptibility χ of a single crystal of $Tm_5Si_2Ge_2$ in the low-temperature region. The magnetic susceptibility was measured upon heating at H=100 Oe with a magnetic field aligned parallel to the b crystallographic axis and ac plane, i.e., χ_b and $\chi_{in\text{-}plane}$, respectively. The zero magnetic field cooled and field-cooled samples showed similar magnetic susceptibilities. χ_b showed a distinct peak at 8.2 K due to antiferromagnetic ordering. Below T_N, χ_b approached zero, and then deviated upward at 7 K. On the other hand, the $\chi_{in\text{-}plane}$ increased with decreasing temperature, flatted at T_N, and again increased below 7 K. This behavior of the magnetic susceptibility approaching zero in χ_b and flatting in the $\chi_{in\text{-}plane}$ immediately below T_N are observed in conventional

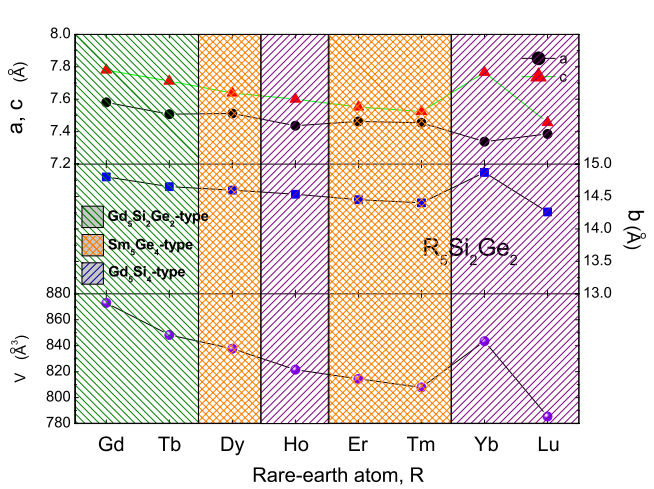

FIG. 3. (Color online) Variation of the lattice parameters of $R_5Si_2Ge_2$ with R=Gd through to Lu.

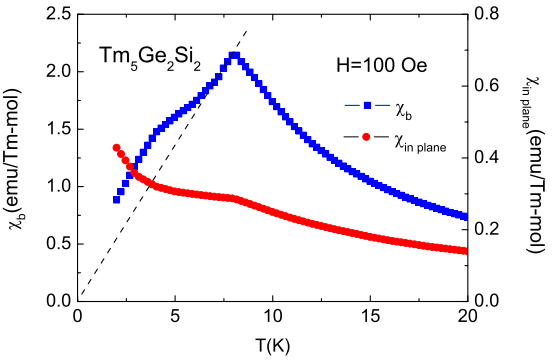

FIG. 4. (Color online) Temperature dependence of the dc magnetic susceptibility of a $Tm_5Si_2Ge_2$ single crystal for the $H\|b$ axis and $H\|ac$ plane in low-temperature regions. The dashed line is one fitted linearly in temperature regions between 7 K and T_N.

antiferromagnetic single crystals. This similarity suggests that the magnetic moments of $Tm_5Si_2Ge_2$ below T_N are coupled antiferromagnetically along the b axis. The increase in the $\chi_{in\text{-}plane}$ below 7 K might be due to the magnetic moment coupled ferromagnetically in the plane, which will be discussed in the section reporting the ac magnetic susceptibility. Such antiferromagnetism was proposed by Landau for layered antiferromagnetic materials, in which the magnetic moments in ferromagnetically ordered layers alternate from layer to layer.[31] In Gd_5Ge_4 the antiferromagnetism proposed by Landau was also observed at T_N=128 K, and the strength of the exchange interactions for antiferromagnetism and ferromagnetism were equal.[32] However, there was anisotropy in the strength of the exchange interactions in $Tm_5Si_2Ge_2$.

To prove our claim regarding the layered magnetic ordering observed in $Tm_5Si_2Ge_2$ the ac magnetic susceptibilities were measured as a function of temperature at different frequencies (Fig. 5). χ_b' is similar to the dc magnetic susceptibility. There was no frequency dependence in the χ_b' near the magnetic ordering, which suggests that the anomalies are caused by long-range magnetic orderings. In χ_b'' below T_N, there was no peak structures suggesting ferromagnetic order. The $\chi_{in\text{-}plane}'$ is also similar to the dc magnetic susceptibility. The $\chi_{in\text{-}plane}''$ shows a peak at approximately 7 K, which is different from the feature observed in χ_b''. The peak originates from long-range ferromagnetic ordering in the plane below 7 K because the peak in the imaginary part of the magnetic susceptibility is formed by energy losses due to the hysteresis observed in ferromagnetic ordering. This strongly supports the claim of magnetic ordering mentioned above.

Figure 6 shows the temperature dependence of the inverse magnetic susceptibility, $1/\chi$. $1/\chi$ is linearly proportional to the temperature at $T>150$ K, and reflects the Curie-Weiss behavior with a paramagnetic Curie temperatures $\Theta_{p,b}$ $\sim$34 K, which suggests that a ferromagnetic exchange interaction exists in the b-axis direction, and $\Theta_{p,in\text{-}plane}\sim-55$ K, which indicates that an antiferromagnetic exchange interaction acts in the ac planes, at $H\|b$ axis and $H\|ac$ plane, respectively. This is inconsistent with the results from the above-mentioned magnetic structure and thus suggests that the main cause of the anisotropic Θ_p's may be the crystalline electric effect rather than an exchange interaction. The evalu-

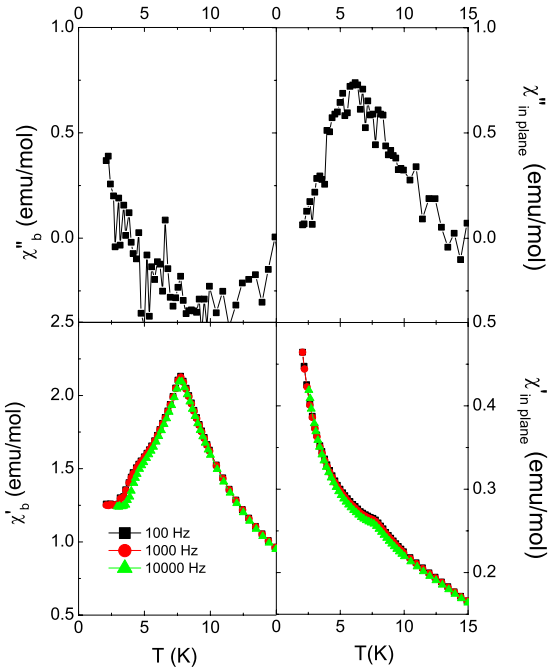

FIG. 5. (Color online) ac magnetic susceptibilities as a function of temperature for different frequencies in $Tm_5Si_2Ge_2$ single crystal.

ated effective magnetic moment, p_{eff}, is equal to $6.8 \pm 0.15 \mu_B$/Tm atom in both directions. The p_{eff} was between that of Tm^{3+} ($p_{eff1}=7.57\mu_B$) and Tm^{2+} ($p_{eff2}=4.54\mu_B$).

As shown in Fig. 7(a), the isothermal magnetization of $Tm_5Si_2Ge_2$ single crystal was measured at $T=2$, 4, and 6 K, which are below the temperature showing ferromagnetic order in the *ac* plane, with an applied magnetic field in the directions parallel to the *b* crystallographic axis and *ac* plane. The magnetization of the $H \| b$ axis, M_b, was much larger than that of the $H \| ac$ plane, $M_{in\text{-}plane}$, in the measured magnetic field regions, which suggests that the *b* axis is the easy axis. In Fig. 7(c), weak upturn in M_b was observed near $H_{cr}=0.5$ T. The existence of the upturn was clearly proved by the plot of dM_b/dH, which is depicted in Fig. 7(b). Remanent-free hysteresis was observed only at $T=2$ K. Hysteresis is generally observed in magnetic materials with

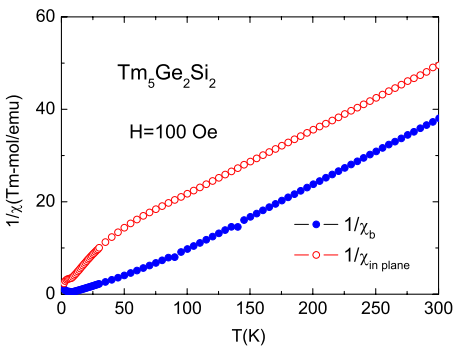

FIG. 6. (Color online) Temperature dependence of the inverse dc magnetic susceptibility of a $Tm_5Si_2Ge_2$ single crystal for the $H \| b$ axis and $H \| ac$ plane.

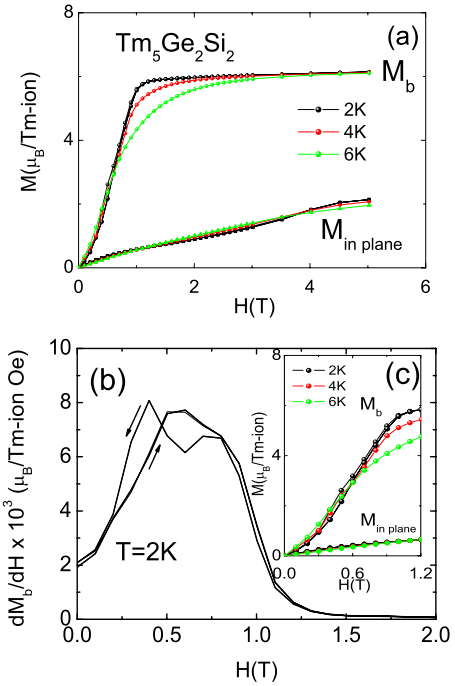

FIG. 7. (Color online) (a) Magnetic field dependence of the magnetization of a $Tm_5Si_2Ge_2$ single crystal for the $H \| b$ axis and $H \| ac$ plane, M_b and $M_{in\text{-}plane}$, respectively, at $T=2$, 4, and 6 K. (b) The derivatives of M_b with respect to the magnetic field at $T=2$ K. (c) M_b and $M_{in\text{-}plane}$ in low magnetic fields.

narrow domain walls.[33–36] In these magnetic materials, the motion of the walls was hindered by pinning centers at low temperatures, giving rise to small magnetization. As the temperature increases, the thermal energy provides the driving force necessary to overcome the barriers created by the pinning centers, leading to an increase in magnetization with increasing temperature.

The M_b remains below $6.1 \pm 0.1 \mu_B$ per Tm ion in a magnetic field of 5 T. The theoretically saturated magnetic moments of Tm^{3+} and Tm^{2+} are given by $gJ=7\mu_B$, M_{3+} and $gJ=4\mu_B$, M_{2+}, respectively, where g is the gyromagnetic ratio and J is the total angular-momentum quantum number. The measured value is intermediate between M_{3+} and M_{2+}. The $M_{in\text{-}plane}$ in the *ac* plane increases slowly with increasing magnetic field with no distinct change in H_{cr}.

The upturn at H_{cr} may be due to a metamagnetic transition caused by flipped magnetic moments in the *ac* plane considering the magnetic structure of $Tm_5Si_2Ge_2$ proposed in the magnetic susceptibility result. However, as an origin of the upturn the progressive rotation of magnetic moments toward the *b* axis or even a spin-flop transition as observed in Gd_5Ge_4,[32] cannot be excluded because canted antiferromagnetic order can form below T_N considering the small saturated magnetic moments. Therefore, a more progressive study is needed.

The specific heat of $Tm_5Si_2Ge_2$ single crystal was measured upon heating in various magnetic fields ranging from 0 to 9 T, which is shown in Fig. 8. The magnetic field was applied parallel to the *b* crystallographic axis. The antiferromagnetic transition observed at $T_N=8.0$ K in the magnetic susceptibility measurements taken at $H=100$ Oe is indicated

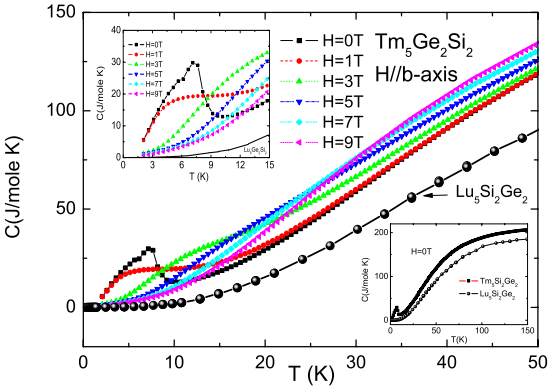

FIG. 8. (Color online) Temperature dependence of the specific heats, C, of a $Tm_5Si_2Ge_2$ single crystal in various magnetic fields for the $H \| b$ axis and $Lu_5Si_2Ge_2$ up to 50 K to see the broad shoulder, which shifts to a higher temperature with increasing H. The left inset shows the specific heat in low-temperature regions to see the peak due to the magnetic transition. The right inset shows the specific heat for whole measured temperature range for comparison of the specific heat of $Tm_5Si_2Ge_2$ with $Lu_5Si_2Ge_2$.

by a sharp peak at 7.7 K in the specific-heat measurements at $H=0$ T. The midpoint temperature (8 K) of the peak in the specific-heat curve is equal to T_N. When $H>1$ T, the sharp peak becomes a broad shoulder and shifts to a higher temperature with further increases in H. To demonstrate this feature distinctly, the phonon part in the specific heat of $Tm_5Si_2Ge_2$ was excluded using the specific heat of the nonmagnetic $Lu_5Si_2Ge_2$. Figure 9 shows the magnetic contribution to the specific heat. In the figure, there appears to be several small humps at approximately $T=26$, 33, 42 K, etc. These humps are due to errors occurring when subtracting the specific heat of $Lu_5Si_2Ge_2$, which were measured at rough-temperature intervals. A shoulder was observed at approximately 7 K at $H=1$ T, 12 K at $H=3$ T, 18 K at $H=5$ T, 28 K at $H=7$ T, and 35 K at $H=9$ T. These shoulders were formed by a Schottky anomaly due to excitation between the crystal-field splitting states, which are divided by the Zeeman effect under internal magnetic fields induced by ferromagnetism as well as by an applied magnetic

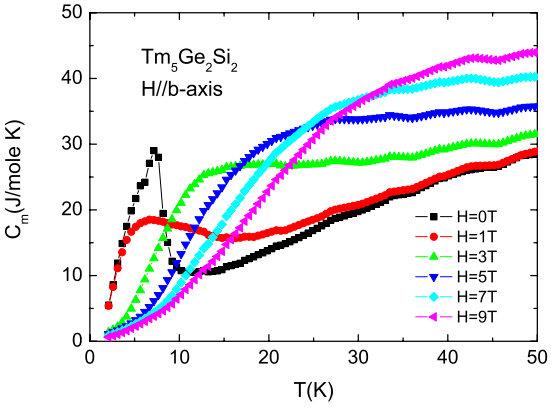

FIG. 9. (Color online) Temperature dependence of the magnetic contribution (C_m) to specific heats of a $Tm_5Si_2Ge_2$ single crystal in various magnetic fields for the $H \| b$ axis.

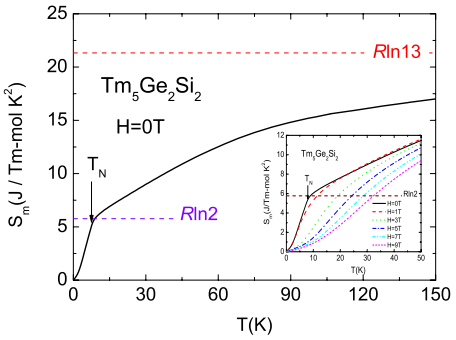

FIG. 10. (Color online) Temperature dependence of the magnetic contribution (S_m) to the entropy of a $Tm_5Si_2Ge_2$ single crystal at $H=0$ T. R ln 13 and R ln 2 are the full entropies of Tm^{+3} and the entropy of a doublet ground state, respectively. The inset shows the entropy under magnetic fields.

field.[37–39] A weak anomaly was observed at 6 K in the specific heat curve at only $H=0$ T, as shown in the inset in Fig. 8. This is consistent with the result of magnetic structure mentioned above. Figure 10 shows the magnetic entropy per Tm mole evaluated from the integral of the magnetic contribution to the specific heat divided by temperature. The magnetic entropy at $H=0$ T was nearly recovered to R ln 2 at T_N. This suggests that the ground state is a doublet considering the low symmetry of its crystal structure. In the high-temperature regions, the magnetic entropy was saturated to approximately 17.5 J/Tm-mol K^2, which is much smaller than the full entropy for Tm^{3+} ions, R ln 13. This is due to the reduced magnetic moment observed in the magnetic susceptibility and magnetization. The magnetic entropy in $H>0$ T approaches the value at $H=0$ T in the high-temperature region. The entropy decreases with increasing magnetic field across all temperatures due to the Zeeman effect.

However, it is unclear why the magnetic moment is reduced. Decreases in the magnetic moments of Tm ions might arise from the mixed-valence state, spin frustration, the Kondo effect, etc. Assuming that there are two distinct Tm valence states in the lattice, the fraction of each ion can be estimated from the experimentally determined effective magnetic moment using the following equation: $p_{eff}=[\alpha p_{eff1}^2+(1-\alpha)p_{eff2}^2]^{1/2}$, where α is the fraction of Tm^{3+} ions. Solving with respect to α, the fraction of Tm^{3+} and Tm^{2+} ions in the unit cell was 0.70 ± 0.05 and 0.30 ± 0.05, respectively. The fraction of each ion present can be estimated from the magnetization in the magnetically ordered state using the following equation: $M=[\alpha M_{3+}+(1-\alpha)M_{2+}]$. Solving with respect to α, the fraction of Tm^{3+} and Tm^{2+} ions in the unit cell was 0.70 ± 0.03 and 0.30 ± 0.03, respectively. The value of α obtained from the saturating magnetic moment is equal to that obtained from the above-mentioned effective magnetic moment. However, the mixed-valence state differs from the result of the change in lattice constant.

The Tm $4d$ and $4p$ XPS spectra of $Tm_5Si_2Ge_2$ were measured to confirm the mixed-valence state in more detail as shown in Fig. 11. The XPS spectra of TmS and TmTe at the same core levels are also plotted as a reference for the Tm^{3+} and Tm^{2+} spectra, respectively. The Tm $4d$ and $4p$ XPS

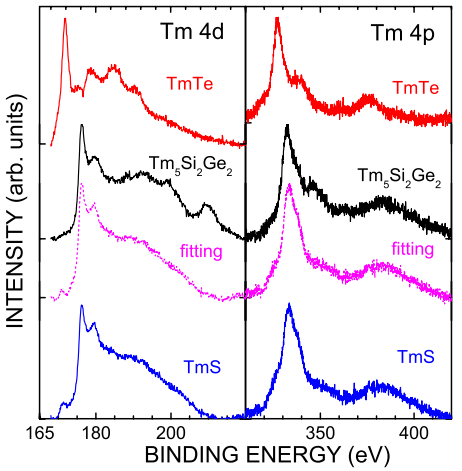

FIG. 11. (Color online) Tm $4d$ and $4p$ XPS spectra of $Tm_5Si_2Ge_2$ and the reference materials, TmS and TmTe measured at $T=20$ K. The fitting results using the linear combination of $1.1I_{TmS}(E)-0.1I_{TmTe}(E)$ are also plotted.

spectra of TmS have shoulders at binding energies of 172 eV and 325 eV, respectively, which originate from the Tm^{2+} state appearing in the XPS spectra of TmTe. These spectral features are consistent with the mixed-valence nature of TmS.[30] In $Tm_5Si_2Ge_2$, the mean valence is almost trivalent compared to TmS because the Tm^{2+} $4d$ peaks do not appear in the Tm $4d$ and $4p$ XPS spectra. The Tm $4d$ and $4p$ XPS spectra of $Tm_5Si_2Ge_2$ can be fitted by a linear combination of the XPS spectra of TmS and TmTe using the following function: $I_{Tm_5Si_2Ge_2}(E)=\alpha I_{TmS}(E)+(1-\alpha)I_{TmTe}(E)$. Here $I_{sample}(E)$ indicates the XPS spectrum and α, which is the fraction of TmS, becomes 1.1 ± 0.1. Since the mean valences of Tm ions in TmS and TmTe are 2.8 and 2.0, respectively,[29] the mean valence of $Tm_5Si_2Ge_2$, z, was estimated to be approximately 2.9 ± 0.1 using the function $z=0.8\alpha+2.0$. Therefore, the mean valence of Tm ions in $Tm_5Si_2Ge_2$ evaluated from the XPS spectra was almost trivalent, which is consistent with the change in unit-cell volume. The change in the lattice constants and XPS are more powerful than the magnetic susceptibility and magnetization because the former is the result observed directly from a mixed valence. In this context, the reduced magnetic moment of Tm ions in $Tm_5Si_2Ge_2$ is not due to the mixed-valence state.

Spin frustration is often observed in triangular, Kagome, and pyrochlore crystal structures. $Tm_5Si_2Ge_2$ does not contain these structures, hence spin frustration can be excluded.

On the other hand, the phenomenon, where the conduction electrons strongly couple with the f-electron spin in the opposite direction by a c-f interaction is known as the Kondo effect. The Kondo effect often causes a decrease in magnetic moment and magnetic entropy. To confirm the correlation between these phenomena and the Kondo effect, this study measured the electrical resistivity of $Tm_5Si_2Ge_2$ and $Lu_5Si_2Ge_2$, which does not contain $4f$ electrons and is a reference for examining magnetic transport in $Tm_5Si_2Ge_2$. Figure 12 shows their electrical resistivity. $Lu_5Si_2Ge_2$ showed a normal metallic temperature dependence, while $Tm_5Si_2Ge_2$ showed two anomalies below 10 K and approximately 200

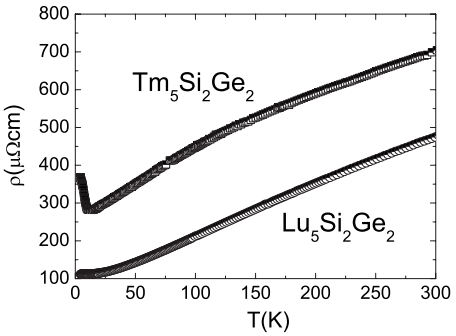

FIG. 12. Temperature dependence of the electrical resistivity of a $Tm_5Si_2Ge_2$ single crystal and $Lu_5Si_2Ge_2$ polycrystal.

K. To observe the anomalies in detail, the electrical resistivity of $Lu_5Si_2Ge_2$ was subtracted from that of $Tm_5Si_2Ge_2$. The result is shown in Fig. 13. The anomalies revealed a log T dependence. This log T behavior is characteristic of the Kondo effect. The log T behavior observed in the low-temperature regions begins from near T_N. In addition, the magnetic entropy of $Tm_5Si_2Ge_2$ recovered to the full entropy of the ground doublet at T_N. This suggests that the ground doublet state, which arises from crystalline electric field (CEF) splitting for the Hund's rule ground state of $J=6$, is unaffected by the Kondo effect, whereas the excited states near the ground state are. The log T behavior in the high-temperature regions is due to the Kondo effect for more excited CEF states. The Kondo temperature (T_K) was estimated to be higher than 200 K according to the Kondo model. The high T_K interrupts the recovery of magnetic entropy at high temperatures, as mentioned above. The magnetic moments of the excited states screened by the Kondo effect should cause a lower decrease in effective magnetic moment and magnetization. The Kondo effect is caused by hybridization between the conduction electrons and $4f$ electrons. The strength of hybridization depends on the overlap of their wave functions. When the excited crystal-field orbitals have a higher overlap with orbitals of the $5d$ conduction electron than the ground orbits, the Kondo effect due to the excited states dominates. This has been reported in Ce monopnictides.[40]

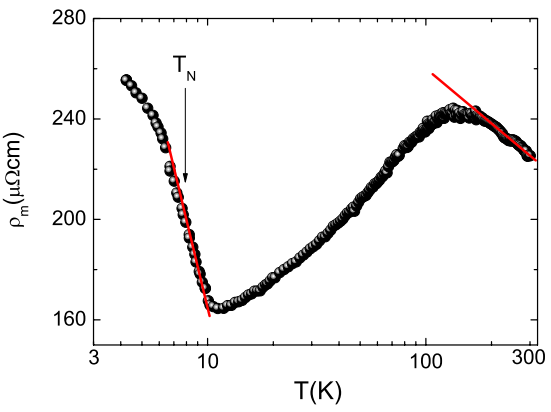

FIG. 13. (Color online) Temperature dependence of the magnetic resistivity of $Tm_5Si_2Ge_2$ subtracting the resistivity of $Lu_5Si_2Ge_2$.

IV. CONCLUSION

$Tm_5Si_2Ge_2$ crystallizes in an orthorhombic Sm_5Ge_4-type structure at 300 K. Long-range antiferromagnetic order coupled along the *b* crystallographic axis was observed below T_N=8.01 K. Below approximately 7 K the antiferromagnetic magnetic moments coupled along the *b* crystallographic axis remain and the magnetic moments in the *ac* crystallographic plane are coupled ferromagnetically. The decrease in magnetic moment and magnetic entropy, and a $-\log T$ dependence in electrical resistivity were observed in the high-temperature regions due to the Kondo effect on an excited crystal-field states. Competition between the Kondo effect and magnetic order plays an important role in $Tm_5Si_2Ge_2$.

ACKNOWLEDGMENT

This study was performed for the Nuclear R&D Programs funded by the Ministry of Science & Technology (MOST) of Korea.

*yskwon@skku.ac.kr

[1] V. K. Pecharsky and K. A. Gschneidner, Jr., Phys. Rev. Lett. **78**, 4494 (1997).
[2] V. K. Pecharsky and K. A. Gschneidner, Jr., Appl. Phys. Lett. **70**, 3299 (1997).
[3] L. Morellon, P. A. Algarabel, M. R. Ibarra, J. Blasco, B. Garcia-Landa, Z. Arnold, and F. Albertini, Phys. Rev. B **58**, R14721 (1998).
[4] W. Choe, V. K. Pecharsky, A. O. Pecharsky, K. A. Gschneidner, Jr., V. G. Young, Jr., and G. J. Miller, Phys. Rev. Lett. **84**, 4617 (2000).
[5] E. M. Levin, V. K. Pecharsky, and K. A. Gschneidner, Jr., Phys. Rev. B **60**, 7993 (1999).
[6] L. Tan, A. Kreyssig, J. W. Kim, A. I. Goldman, R. J. McQueeney, D. Wermeille, B. Sieve, T. A. Lograsso, D. L. Schlagel, S. L. Budko, V. K. Pecharsky, and K. A. Gschneidner, Jr., Phys. Rev. B **71**, 214408 (2005).
[7] J. M. Cadogan, D. H. Ryan, Z. Altounian, H. B. Wang, and I. P. Swainson, J. Phys.: Condens. Matter **14**, 7191 (2002).
[8] G. H. Rao, Q. Huang, H. F. Yang, D. L. Ho, J. W. Lynn, and J. K. Liang, Phys. Rev. B **69**, 094430 (2004).
[9] C. Ritter, L. Morellon, P. A. Algarabel, C. Magen, and M. R. Ibarra, Phys. Rev. B **65**, 094405 (2002).
[10] L. Morellon, C. Ritter, C. Magen, P. A. Algarabel, and M. R. Ibarra, Phys. Rev. B **68**, 024417 (2003).
[11] C. Magen, C. Ritter, L. Morellon, P. A. Algarabel, and M. R. Ibarra, J. Phys.: Condens. Matter **16**, 7427 (2004).
[12] J. M. Cadogan, D. H. Ryan, Z. Altounian, X. Liu, and I. P. Swainson, J. Appl. Phys. **95**, 7076 (2004).
[13] V. O. Garlea, J. L. Zarestky, C. Y. Jones, L. L. Lin, D. L. Schlagel, T. A. Lograsso, A. O. Tsokol, V. K. Pecharsky, K. A. Gschneidner, Jr., and C. Stassis, Phys. Rev. B **72**, 104431 (2005).
[14] C. Ritter, C. Magen, L. Morellon, P. A. Algarabel, M. R. Ibarra, V. K. Pecharsky, A. O. Tsokol, and K. A. Gschneidner, Jr., J. Phys.: Condens. Matter **18**, 3937 (2006).
[15] L. Morellon, C. Magen, P. A. Algarabel, M. R. Ibarra, and C. Ritter, Appl. Phys. Lett. **79**, 1318 (2001).
[16] Kyunghan Ahn, A. O. Tsokol, Yu. Mozharivskyj, K. A. Gschneidner, Jr., and V. K. Pecharsky, Phys. Rev. B **72**, 054404 (2005).
[17] A. O. Pecharsky, K. A. Gschneidner, Jr., V. K. Pecharsky, D. L. Schlagel, and T. A. Lograsso, Phys. Rev. B **70**, 144419 (2004).
[18] A. O. Pecharsky, V. K. Pecharsky, and K. A. Gschneidner, Jr., J. Alloys Compd. **379**, 127 (2004).
[19] H. F. Yang, G. H. Rao, W. G. Chu, G. Y. Liu, Z. W. Ouyang, and J. K. Liang, J. Alloys Compd. **334**, 131 (2002).
[20] H. F. Yang, G. H. Rao, G. Y. Liu, Z. W. Ouyang, W. F. Liu, X. M. Feng, W. G. Chu, and J. K. Liang, J. Alloys Compd. **361**, 113 (2003).
[21] H. F. Yang, G. H. Rao, W. G. Chu, G. Y. Liu, Z. W. Ouyang, and J. K. Liang, J. Alloys Compd. **339**, 189 (2002).
[22] H. F. Yang, G. H. Rao, G. Y. Liu, Z. W. Ouyang, W. F. Liu, X. M. Feng, W. G. Chu, and J. K. Liang, J. Magn. Magn. Mater. **263**, 146 (2003).
[23] H. F. Yang, G. H. Rao, G. Y. Liu, Z. W. Ouyang, W. F. Liu, X. M. Feng, W. G. Chu, and J. K. Liang, J. Alloys Compd. **346**, 190 (2002).
[24] L. Morellon, Z. Arnold, C. Magen, C. Ritter, O. Prokhnenko, Y. Skorokhod, P. A. Algarabel, M. R. Ibarra, and J. Kamarad, Phys. Rev. Lett. **93**, 137201 (2004).
[25] V. V. Ivtchenko, V. K. Pecharsky, and K. A. Gschneidner, Jr., Adv. Cryog. Eng. **46A**, 405 (2000).
[26] K. A. Gschneidner, Jr., V. K. Pecharsky, A. O. Pecharsky, V. V. Ivtchenko, and E. M. Levin, J. Alloys Compd. **303-304**, 214 (2000).
[27] G. S. Smith, Q. Johnson, and A. G. Tharp, Acta Crystallogr. **22**, 269 (1967).
[28] G. S. Smith, A. G. Tharp, and Q. Johnson, Acta Crystallogr. **22**, 940 (1967).
[29] K. G. Nath, Y. Ufukutepe, S. Kimura, Y. Haruyama, T. Kinoshita, T. Matsumura, T. Suzuki, H. Ogasawara, and A. Kotani, J. Phys. Soc. Jpn. **72**, 1792 (2003).
[30] E. Bucher, K. Andres, F. J. di Salvo, J. P. Maita, A. C. Gossard, A. S. Cooper and G. W. Hull, Jr., Phys. Rev. B **11**, 500 (1975).
[31] K. Held, M. Ulmke, N. Blumer, and D. Vollhardt, Phys. Rev. B **56**, 14469 (1997).
[32] E. M. Levin, K. A. Gschneidner, Jr., T. A. Lograsso, D. L. Schlagel, and V. K. Pecharsky, Phys. Rev. B **69**, 144428 (2004).
[33] Niraj K. Singh, S. Agarwal, K. G. Suresh, R. Nirmala, A. K. Nigam, and S. K. Malik, Phys. Rev. B **72**, 014452 (2005).
[34] Niraj K. Singh, K. G. Suresh, R. Nirmala, A. K. Nigam, and S. K. Malik, J. Appl. Phys. **101**, 093904 (2007).
[35] J. L. Wang, C. Marquina, M. R. Ibarra, and G. H. Wu, Phys. Rev. B **73**, 094436 (2006).
[36] R. Nirmala, A. V. Morozkin, and S. K. Malik, Phys. Rev. B **75**, 094419 (2007).
[37] J. A. Blanco, D. Gignoux, and D. Schmitt, Phys. Rev. B **43**,

13145 (1991).
[38] M. Bouvier, P. Lethuillier, and D. Schmitt, Phys. Rev. B **43**, 13137 (1991).
[39] R. Mallik and E. V. Sampathkumaran, Phys. Rev. B **58**, 9178 (1998).
[40] H. Takahashi and T. Kasuya, J. Phys. C **18**, 2709 (1985).